SUPPLEMENTARY FIGURE LEGENDS

Suppl. Fig. 1: (A) The NEBD-DCON interval measured in the first (P_0) and second (AB) embryonic divisions for the indicated conditions in a strain expressing GFP-histone H2b and GFP-γ-tubulin. The number of control and Mad2^{MDF-2}-depleted embryos analyzed are indicated in the bars of the graph. Error bars represent the S.E.M. with a 95% confidence interval. The Control values shown for P_0 are the same as those in Figure 1. **(B)** Kinetochore-spindle microtubule interactions are unaffected by depletion of Mad1^{MDF-1}. Spindle pole positions were tracked at 10s intervals; different movies were time-aligned with respect to anaphase onset (t=0) and the average value plotted for each time point. Error bars represent the S.E.M. with a 95% confidence interval. Similar results were obtained in Mad2^{MDF-2}, Mad3^{SAN-1} and Mad2^{MDF-2} & Mad3^{SAN-1} co-depleted embryos.

Suppl. Fig. 2: (A) Aurora B^{AIR-2} inhibition does not abrogate the monopolar spindle-induced delay. Aurora B^{AIR-2} (and the entire chromosomal passenger complex) is essential for meiotic chromosome disjunction and cytokinesis in *C. elegans* embryos (e.g. see Oegema et al., 2001). Consequently, Aurora B inhibition by RNAi results in a fertilized one-cell embryo with a highly aberrant genome (no polar bodies are formed) that does not undergo cytokinesis to form a 2-cell embryo (see supplementary movies for Oegema et al. 2001). This phenotype prevents use of the monopolar spindle assay that we developed to study checkpoint signaling. Aurora inhibitors do not work in *C.*

elegans; inhibitor studies are also complicated by the embryo eggshell, which is impermeable.

To overcome the above limitations we utilized a conditional mutation (*or707ts*) in Aurora B^{air-2} identified in a prior study (Severson et al., 2000 *Curr. Biol.* 10(19):1162-71). In this mutant, there is a Proline to Leucine substitution in subdomain XI of the kinase domain that leads to a temperature sensitive loss-of-function phenotype (see Severson et al. 2000 for a thorough characterization). We obtained this mutant and crossed it into a strain expressing GFP::alpha-tubulin and GFP::histone H2b. We then performed fast-acting temperature shifts on a microscope to analyze the consequences of reducing Aurora B activity ***after*** the first cell division was finished (we used cytokinesis failure, a consequence of Aurora B inhibition, as a means to assess efficacy of the temperature shift). We compared the indicated conditions at the restrictive temperature and quantified the NEBD-DCON interval in both AB & P_1 cell divisions. Inhibition of AuroraB^{AIR-2} did not abrogate the monopolar spindle induced delay – co-depletion of Mad3^{SAN-1} eliminated the delay.

(B) *sgo-1(RNAi)* does not abrogate the monopolar spindle-induced delay.

(C) GFP::Mad2^{MDF-2} enrichment at unattached kinetochores is not significantly affected by AuroraB^{AIR-2} RNAi. Unattached kinetochores were generated in the first division using a dsRNA targeting α-tubulin.

Suppl. Fig. 3: (A) The GFP-Mad2^{MDF-2} transgene expressed under control of the *pie-1* promoter causes a monopolar spindle-induced delay in the second division of a strain in which endogenous Mad2^{MDF-2} is absent. The NEBD-DCON intervals measured in the

two different strains (OD215 and OD216) and indicated conditions were normalized relative to the same interval measured in AB cells with bipolar spindles in the deletion mutant strain (OD215). The general sickness and very low brood size of the Mad2$^{mdf\text{-}2}\Delta$ strain, which is partially rescued by the GFP::Mad2$^{MDF\text{-}2}$ transgene (*not shown*), limited analysis of the early embryonic divisions in these experiments. Error bars represent the 95% confidence interval – errors were propagated through the normalization using Graphpad (http://www.graphpad.com/quickcalcs/ErrorProp1.cfm?Format=SEM).

(B) Effect of depleting Mad3$^{SAN\text{-}1}$ or BUB-3 on peak kinetochore levels of GFP-Mad2$^{MDF\text{-}2}$ in AB cells with monopolar spindles. To specifically measure kinetochore-localized GFP::Mad2$^{MDF\text{-}2}$, a subtraction approach, similar to Dammermann et al. (2008), was used. Total fluorescence in the nuclear region (measured by integrating fluorescence intensity in a box surrounding the nucleus after subtracting cytoplasmic background), which included kinetochore-localized fluorescence, was measured for each of the indicated conditions and also for *zyg-1+rod-1(RNAi)*, where kinetochore accumulation of Mad2$^{MDF\text{-}2}$ is inhibited. Each sequence was normalized relative to the total fluorescence at NEBD and the values measured at each time point for the *zyg-1+rod-1(RNAi)* were subtracted from the same time points of the indicated conditions to specifically isolate kinetochore-specific GFP::Mad2$^{MDF\text{-}2}$ fluorescence. The peak of GFP::Mad2$^{MDF\text{-}2}$ accumulation was slightly earlier relative to NEBD in Mad3$^{SAN\text{-}1}$ depletion, in comparison to the monopolar control, but the magnitude of the peak was indistinguishable from the monopolar control. BUB-3 depletion resulted in peak fluorescence approximately half that of the monopolar control. Errors were propagated throughout the analysis and the 95% confidence interval is plotted.

Suppl. Fig. 4: (A) The GFP::Mad3^{SAN-1} transgene expressed under control of the *pie-1* promoter causes a monopolar spindle-induced delay in the second division of a strain in which endogenous Mad3^{SAN-1} is absent. The NEBD-DCON intervals measured after *zyg-1(RNAi)* were normalized relative to the same interval measured without *zyg-1(RNAi)* in each strain. Error bars represent the 95% confidence interval – errors were propagated through the normalization using Graphpad (http://www.graphpad.com/quickcalcs/ErrorProp1.cfm?Format=SEM).

(B) The diffuse nuclear region fluorescence of GFP::Mad3^{SAN-1} is eliminated by Mad3^{san-1}*(RNAi)*. Scale bar = 5 μm.

Suppl. Fig. 5: (A) Localization of endogenous BUB-3 in a one-cell embryo with a bipolar spindle. *bub-3(RNAi)* eliminates the observed kinetochore localization. Scale bar = 10 μm.

(B) Accumulation of GFP::BUB-3 at kinetochores on chromosomes associated with monopolar spindles is eliminated by *bub-3(RNAi)*. Scale bar = 5 μm.

(C) GFP::BUB-3 kinetochore localization is independent of the NDC-80 complex.

(D) Mad1^{MDF-1} is required for the monopolar spindle-induced delay in the GFP-BUB-3 strain.

SUPPLEMENTARY TABLES

Supplementary Table 1. Summary of supplemental movies.

In all videos, the anterior of the embryo is to the left and the posterior of the embryo is to the right. Movies of the same worm strain were recorded with identical acquisition parameters and were scaled equivalently. Playback speed is 6 frames per second.

Video #	**Strain**	**Fluorescent Markers**	**RNAi**	
1	TH32	GFP::histone H2b; GFP::γ-tubulin First (P0 cell) divisions	None (control)	*zyg-1*
			blank	*zyg-1*+ Mad2^{mdf-2}
2	TH32	GFP::histone H2b; GFP::γ-tubulin Second (AB cell) divisions	None (control)	*zyg-1*
			blank	*zyg-1*+ Mad2^{mdf-2}
3	OD95	GFP::PH; mCherry::histone H2b First (P0 cell) divisions	None (control)	*zyg-1*
			blank	*zyg-1* +Mad2^{mdf-2}
4	OD95	GFP::PH; mCherry::histone H2b Second (AB cell) divisions	None (control)	*zyg-1*
			blank	*zyg-1* +Mad2^{mdf-2}
5	OD110	GFP::Mad2^{MDF-2}; mCherry::histone H2b	None (control)	*zyg-1*
6	OD110	GFP::Mad2^{MDF-2}; mCherry::histone H2b	*zyg-1 (same movie as in #5)*	*zyg-1*+ Mad1^{mdf-1}
7	OD110	GFP::Mad2^{MDF-2}; mCherry::histone H2b	*zyg-1 (same movie as in #5)*	*zyg-1+bub-3*
8	OD110	GFP::Mad2^{MDF-2}; mCherry::histone H2b	*zyg-1 (same movie as in #5)*	*zyg-1*+Mad3^{san-1}
9	OD110 OD207	GFP::Mad2^{MDF-2}; mCherry::histone H2b / GFP::Mad2^{MDF-2}; mCherry::histone H2b,*san-1Δ*	*zyg-1*+ Mad3^{san-1} *(same movie as in #8)*	*zyg-1*
10	OD197	GFP::Mad3^{SAN-1}; mCherry::histone H2b	None (control)	*zyg-1*

11	OD197	OD208	GFP::Mad3^{SAN-1}; mCherry::histone H2b	GFP::Mad3^{SAN-1}; mCherry::histone H2b, Mad3$^{san-1\Delta}$	*zyg-1 (same movie as in #10)*	*zyg-1*
12	OD197		GFP::Mad3^{SAN-1}; mCherry::histone H2b		*zyg-1 (same movie as in #10)*	*zyg-1+bub-3*
13	OD197		GFP::Mad3^{SAN-1}; mCherry::histone H2b		*zyg-1 (same movie as in #10)*	*zyg-1+* Mad1^{mdf-1}
					zyg-1+bub-3 (same movie as in #12)	*zyg-1+bub-1*
14	OD196		GFP::BUB-3; mCherry::histone H2b		None (control)	*zyg-1*
15	OD196		GFP::BUB-3; mCherry::histone H2b		*zyg-1 (same movie as in #14)*	*zyg-1+bub-1*
16	OD196		GFP::BUB-3; mCherry::histone H2b		*zyg-1 (same movie as in #14)*	*zyg-1+rod-1*

A

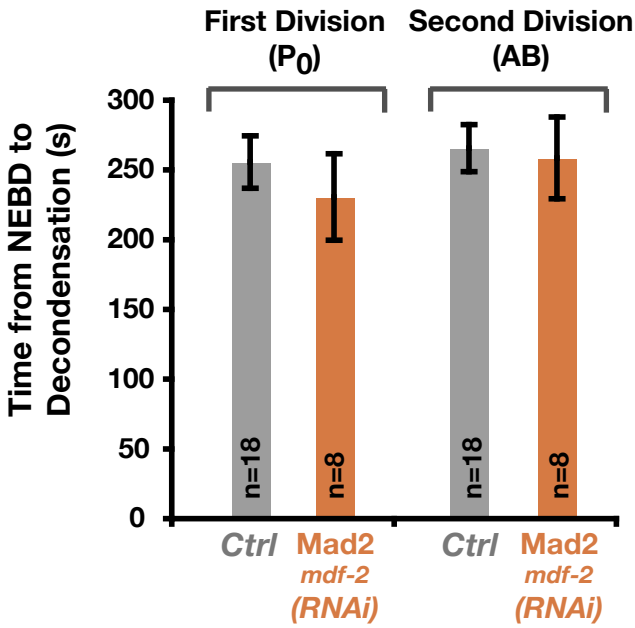
First Division
(P0)
Second Division
(AB)
Time from NEBD to
Decondensation (s)
300
250
200
150
100
50
0
n=18
n=8
n=18
n=8
Ctrl
Mad2
mdf-2
(RNAi)
Ctrl
Mad2
mdf-2
(RNAi)

B

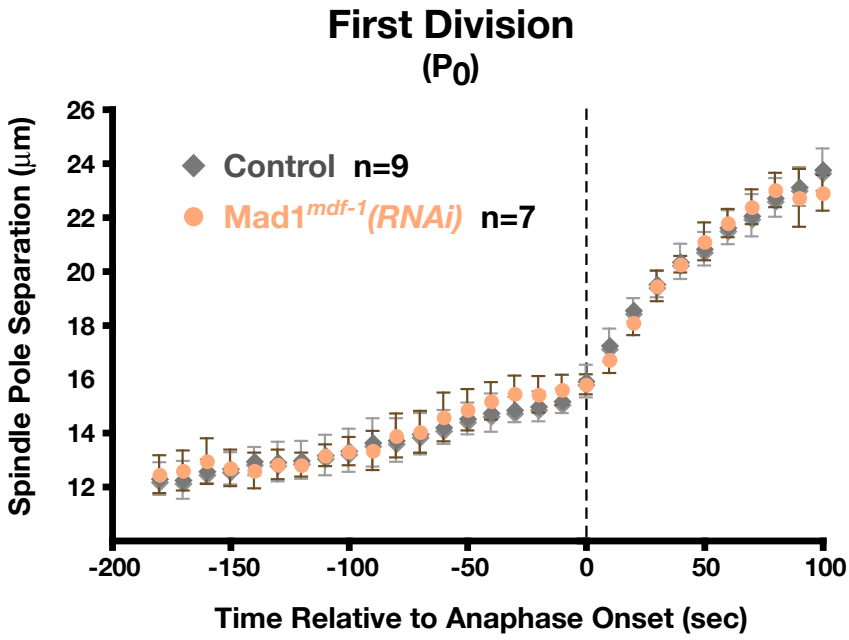
First Division
(P0)
Spindle Pole Separation (μm)
26
24
22
20
18
16
14
12
Control n=9
Mad1mdf-1(RNAi) n=7
-200
-150
-100
-50
0
50
100
Time Relative to Anaphase Onset (sec)

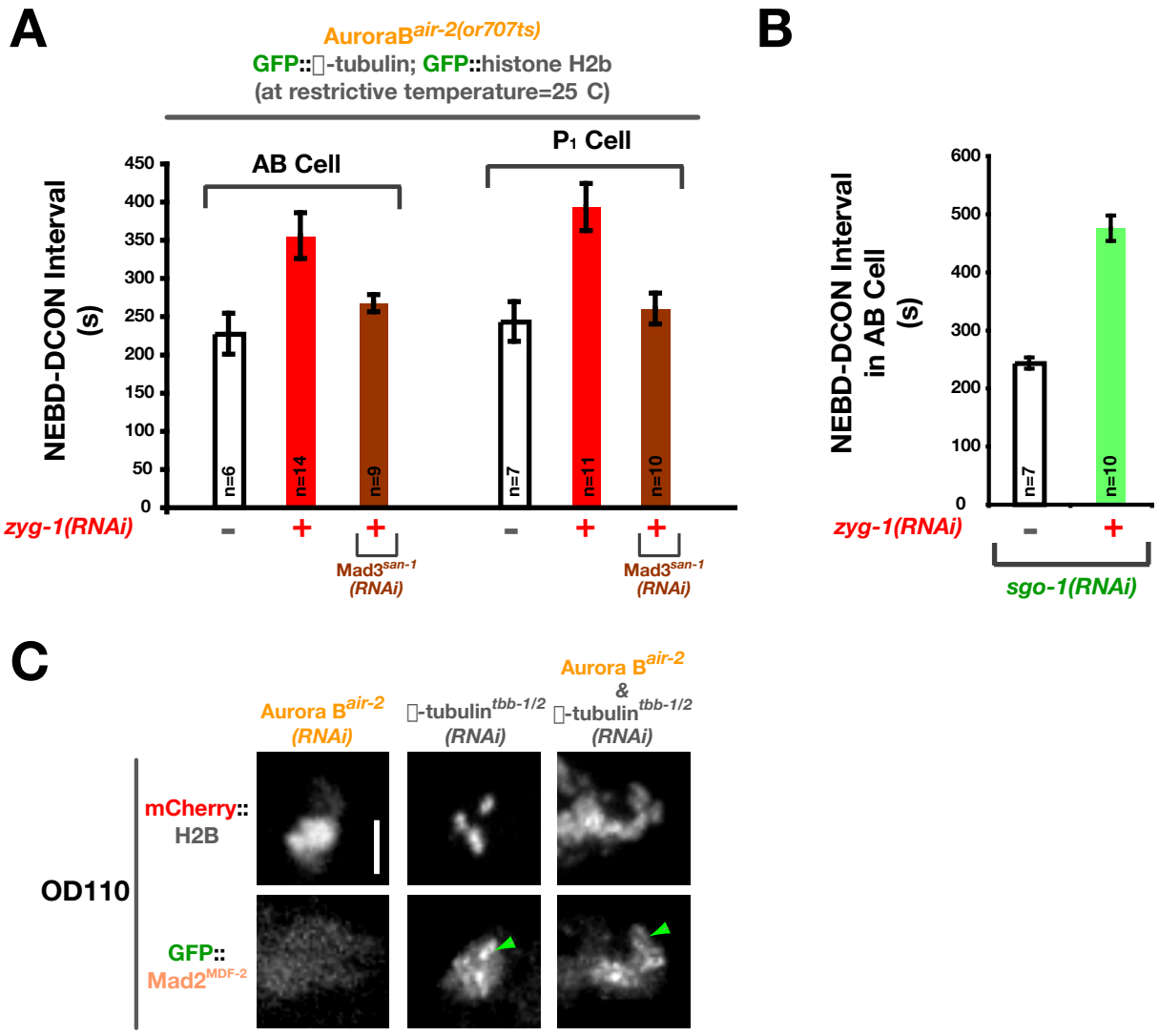
A
AuroraB air-2(or707ts)
GFP::-tubulin; GFP::histone H2b
(at restrictive temperature=25 C)
AB Cell
P1 Cell
NEBD-DCON Interval (s)
450
400
350
300
250
200
150
100
50
0
n=6
n=14
n=9
n=7
n=11
n=10
zyg-1(RNAi)
-
+
+
-
+
+
Mad3san-1 (RNAi)
Mad3san-1 (RNAi)
B
NEBD-DCON Interval in AB Cell (s)
600
500
400
300
200
100
0
n=7
n=10
zyg-1(RNAi)
-
+
sgo-1(RNAi)
C
Aurora Bair-2 (RNAi)
-tubulintbb-1/2 (RNAi)
Aurora Bair-2 & -tubulintbb-1/2 (RNAi)
OD110
mCherry:: H2B
GFP:: Mad2MDF-2

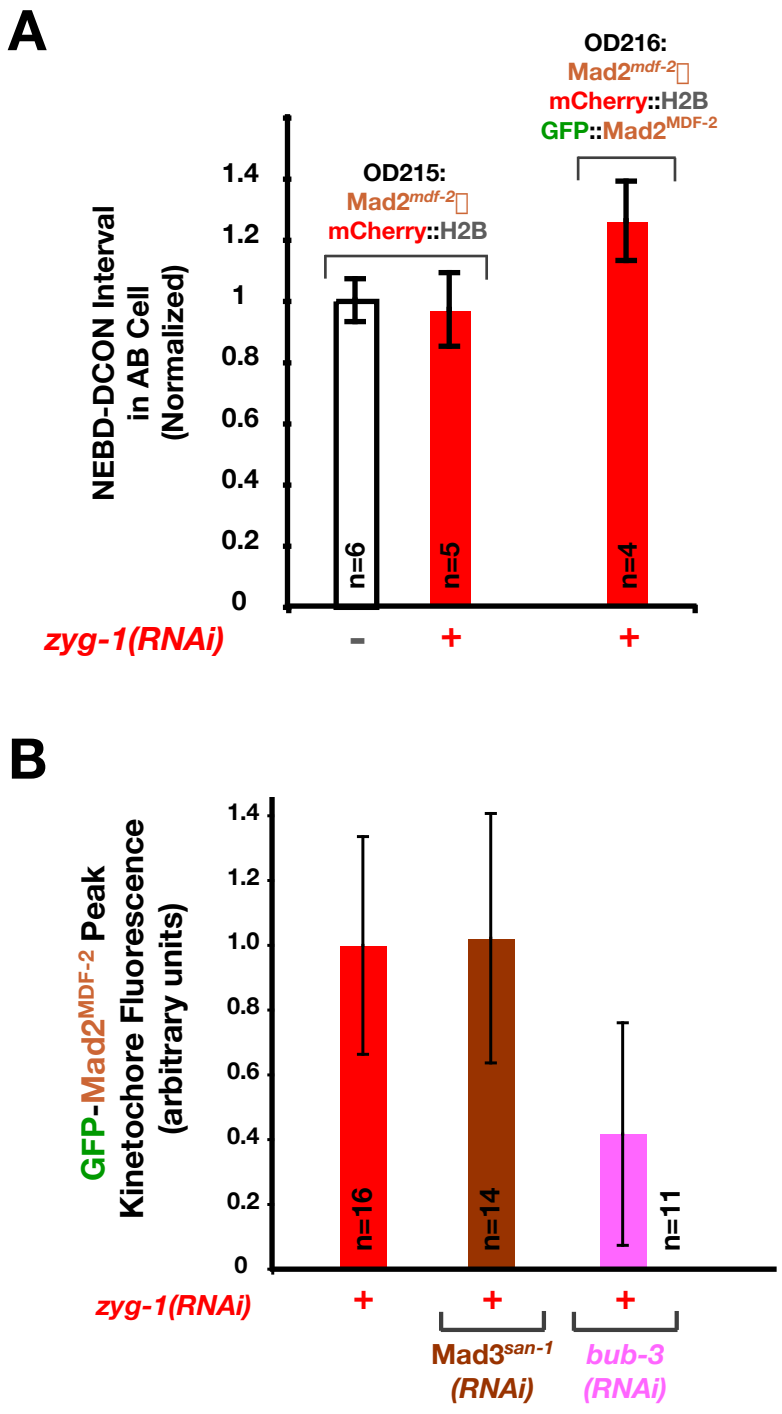
A
OD216:
Mad2mdf-2
mCherry::H2B
GFP::Mad2MDF-2
OD215:
Mad2mdf-2
mCherry::H2B
NEBD-DCON Interval in AB Cell (Normalized)
1.4
1.2
1
0.8
0.6
0.4
0.2
0
n=6
n=5
n=4
zyg-1(RNAi)
-
+
+
B
GFP-Mad2MDF-2 Peak Kinetochore Fluorescence (arbitrary units)
1.4
1.2
1.0
0.8
0.6
0.4
0.2
0
n=16
n=14
n=11
zyg-1(RNAi)
+
+
+
Mad3san-1 (RNAi)
bub-3 (RNAi)

Essex et al. Suppl. Fig. 4

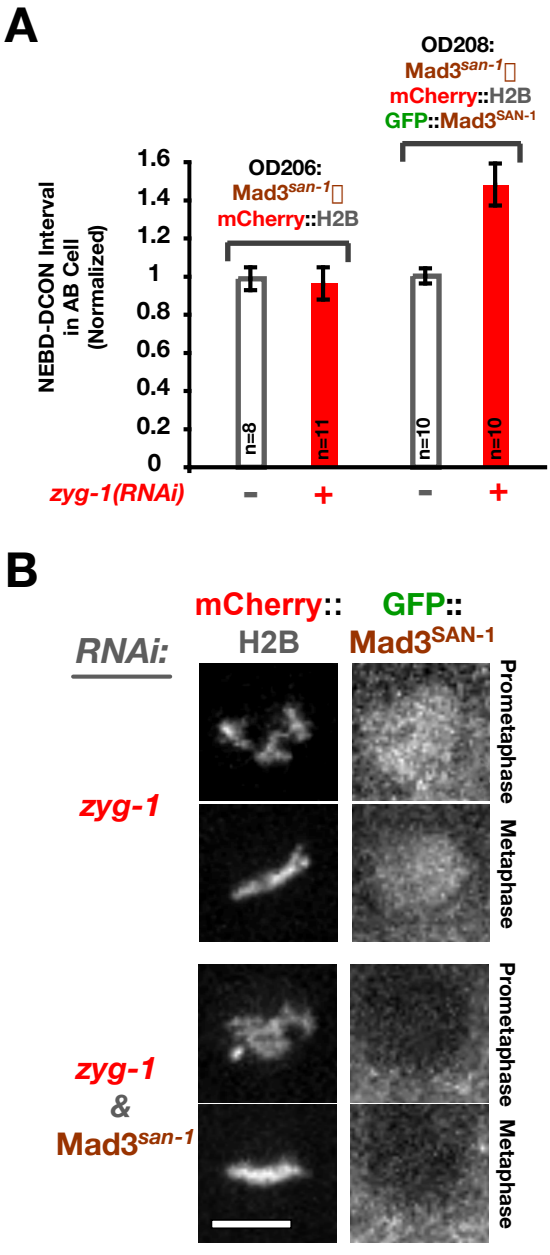

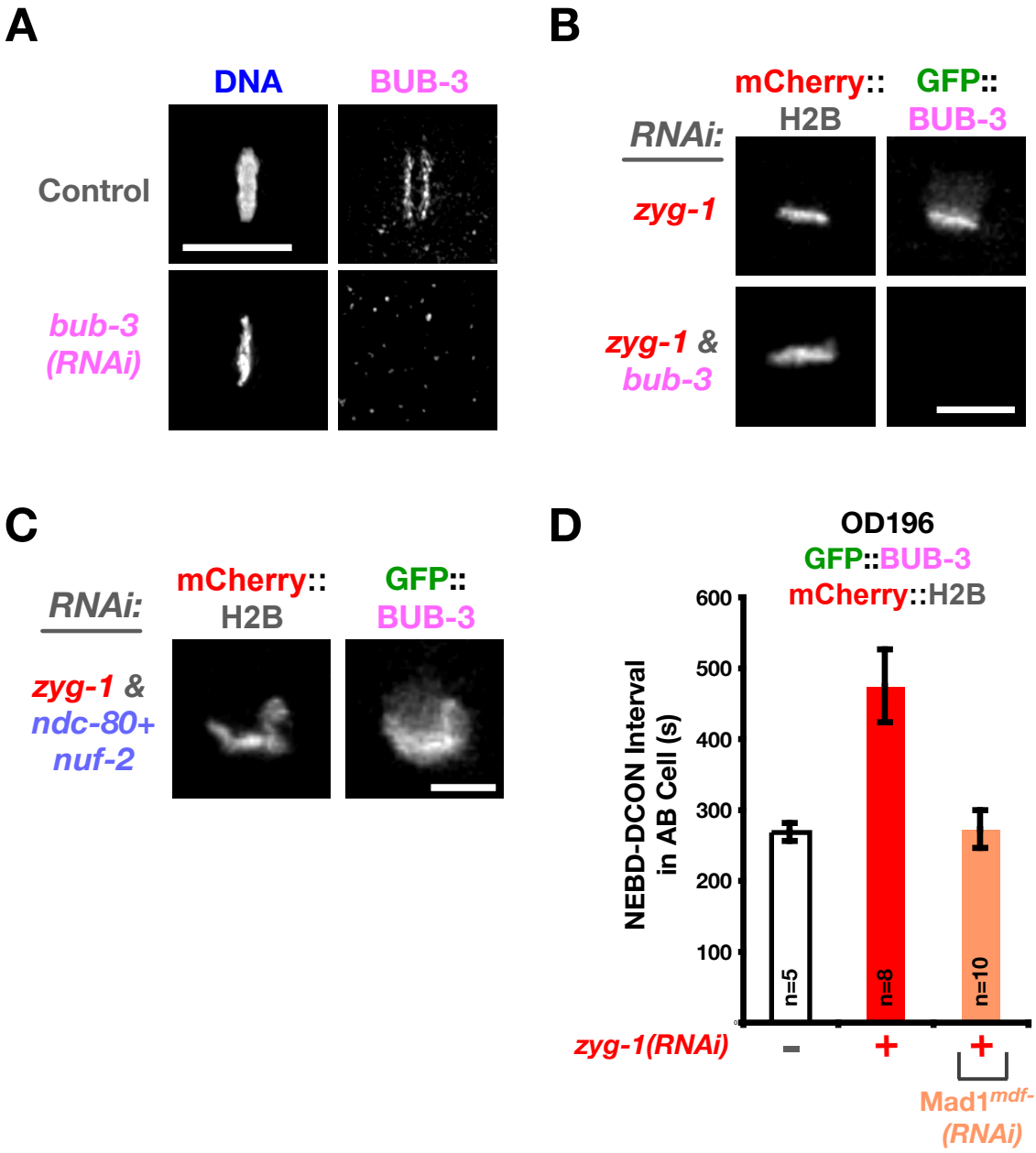
A
DNA
BUB-3
Control
bub-3 (RNAi)
B
mCherry:: H2B
GFP:: BUB-3
RNAi:
zyg-1
zyg-1 & bub-3
C
RNAi:
mCherry:: H2B
GFP:: BUB-3
zyg-1 & ndc-80+ nuf-2
D
OD196
GFP::BUB-3
mCherry::H2B
NEBD-DCON Interval in AB Cell (s)
600
500
400
300
200
100
n=5
n=8
n=10
zyg-1(RNAi)
-
+
+
Mad1mdf-1 (RNAi)